

Generating two-dimensional ferromagnetic charge density waves via external fields


Heng Jin

*Beijing Computational Science Research Center, Beijing 100193, China
and Department of Physics, Beijing Normal University, Beijing 100875, China*

Jiabin Chen

*Key Laboratory of Computational Physical Sciences (Ministry of Education), Institute of Computational Physical Sciences,
State Key Laboratory of Surface Physics, and Department of Physics, Fudan University, Shanghai 200433, China
and Beijing Computational Science Research Center, Beijing 100193, China*

Yang Li

*Beijing Computational Science Research Center, Beijing 100193, China*Bin Shao *College of Electronic Information and Optical Engineering, Nankai University, Tianjin 300350, China*Bing Huang **Beijing Computational Science Research Center, Beijing 100193, China
and Department of Physics, Beijing Normal University, Beijing 100875, China*

(Received 18 March 2022; revised 23 September 2022; accepted 29 September 2022; published 13 October 2022)

Two-dimensional (2D) ferromagnetic charge density waves (CDWs), an exotic quantum state for exploring the intertwining effect between correlated charge and spin orders in the 2D limit, have yet to be discovered under moderate temperatures. Here, we propose a feasible strategy to realize 2D ferromagnetic CDWs under external fields, which is demonstrated in monolayer VSe_2 using first-principles calculations. Under external tensile strain, two ferromagnetic CDWs ($\sqrt{3}\times\sqrt{3}$ and $2\times 2\sqrt{3}$ CDWs) can be generated, accompanied by distinguishable lattice reconstructions of magnetic V atoms. Remarkably, because the driving forces for generating these two ferromagnetic CDWs are strongly spin dependent, fundamentally different from that in conventional CDWs, the $\sqrt{3}\times\sqrt{3}$ and $2\times 2\sqrt{3}$ CDWs can exhibit two dramatically different half-metallic phases under a large strain range, along with either a flat band or a Dirac cone around the Fermi level. Our proposed strategy and material demonstration may provide a feasible way to generate and manipulate the correlation effect between collective charge and spin orders via external fields.

DOI: [10.1103/PhysRevB.106.165112](https://doi.org/10.1103/PhysRevB.106.165112)**I. INTRODUCTION**

The reduced dimensionality in two-dimensional (2D) materials leads to enhanced correlation effects, which is beneficial for generating multiple symmetry-breaking orders. Of particular interest is the coexistence or competition between charge density waves (CDWs) with superconductivity and magnetism in the 2D limit [1–4]. While the coexistence of CDWs and superconductivity has been observed in some 2D transition-metal dichalcogenides (TMDs) [1,2] and consequently stimulated intensive attention in many other correlated systems [5,6], the coexistence of CDWs and ferromagnetism in 2D systems, forming 2D ferromagnetic CDWs, has rarely been experimentally reported yet. Though local magnetic moments exist in the star-of-David (SOD) phase of 1T-TaS₂, a Curie-Weiss temperature of only ~ 0.02 K sug-

gests weak magnetic interactions in this system [7], limiting further applications with coupled spin and charge orders. Fundamentally, these unique time-reversal symmetry-breaking CDWs themselves or in combination with superconductivity and topology may contribute to a series of long-sought physics phenomena, e.g., an unconventional anomalous Hall effect, chiral charge order, and Kondo lattices [5,6,8,9]. Practically, the 100% spin-polarized ferromagnetic CDW, i.e., half-metallic CDW, could be an ideal platform to realize a novel CDW-controlled metal-insulator transition in the single-spin channel for exotic spintronics and information storage [10], beyond the conventional nonmagnetic CDWs [11].

The realization of 2D ferromagnetic CDWs is tacitly accepted to be unlikely, mainly due to the mutually exclusive energy gain accounting for the formation of CDW and ferromagnetism: (i) Forming CDWs usually reduces the density of states (DOS) at the Fermi level (E_F), accordingly decreasing the possibility for forming Stoner itinerant ferromagnetism; (ii) forming ferromagnetism causes the splitting

*bing.huang@csrc.ac.cn

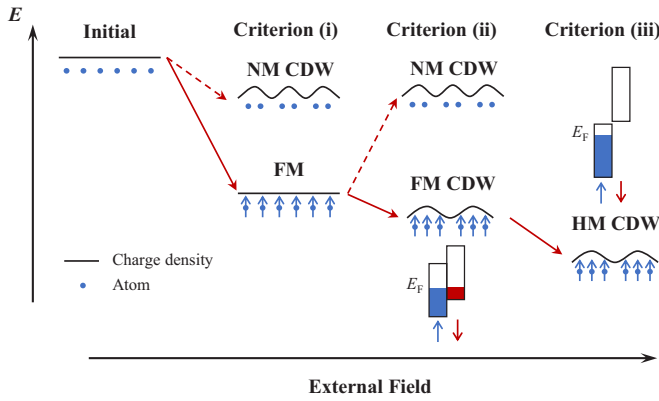


FIG. 1. A strategy for generating ferromagnetic CDWs. Criterion (i) requires the system to hold the ferromagnetic (FM) phase and nonmagnetic (NM) CDW as the ground state and metastable state, respectively. Criterion (ii) represents that an external field may trigger a new FM CDW formation. Criterion (iii) is an additional requirement for half-metallic (HM) CDW formation. See text for more explanation.

of energy bands around E_F , reshaping the topology of Fermi surfaces (FSs) and weakening the condition for FS nesting (FSN), one possible origin of CDWs [12,13]. As a typical example, monolayer (ML) VSe_2 is able to exhibit multiple CDW phases [14–19], room-temperature magnets [20,21], and even possible superconductivity [22]. However, after more than three decades of studies [3,14–24], ferromagnetic CDWs have yet to be observed in VSe_2 . A similar situation is also found in other 2D TMD systems [1–3]. Until now, a feasible strategy to realize 2D ferromagnetic CDW is still lacking, preventing the understanding of new correlation effects between collective charge- and spin-order-induced novel physics phenomena in the monolayer limit.

II. A STRATEGY FOR GENERATING FERROMAGNETIC CDWs

Here, we propose a feasible strategy to realize ferromagnetic CDWs under an external field, following two possible criteria: (i) The system should exhibit a ferromagnetic configuration and its competing nonmagnetic CDW as the ground state and metastable state, respectively, making it a possible platform for realizing different complex ground states (left panel, Fig. 1); (ii) an external field could induce dynamic instability of this ferromagnetic configuration but maintains its total energy lower than that of nonmagnetic CDWs; the dynamic instability increases as the external field increases. Once criteria (i) and (ii) are satisfied, upon a certain external field a sufficiently strong dynamical instability may trigger a new CDW coexisting with ferromagnetic order (middle panel, Fig. 1), as long as the ferromagnetic order can survive the lattice reconstruction. Importantly, during the formation of the ferromagnetic CDW, an additional criterion [criterion (iii)] may be required to form a half-metallic CDW, that is, the major driving force for ferromagnetic CDW formation should be strongly spin dependent. As a result, a significantly different band renormalization could occur in different spin channels, providing a key ingredient for forming half metal-

licity (right panel, Fig. 1). In practice, the 2D systems are ideal platforms to realize this strategy due to their convenience to be applied with various external fields, e.g., strain [25,26], electric [27,28], and irradiation [29,30] fields.

In this paper, using first-principles calculations (see the Methods section in Supplemental Material [31]), we propose that ML- VSe_2 is an ideal platform to generate ferromagnetic CDWs via our strategy. First, ML- VSe_2 holds a ferromagnetic $1T$ phase (nonmagnetic CDWs) as the ground state (metastable states), satisfying criterion (i). Second, under in-plane tensile strain (ϵ), the total energy of the ferromagnetic $1T$ phase continues to be lower than that of nonmagnetic CDWs, but its dynamic instability increases as ϵ increases, satisfying criterion (ii). Therefore, two ferromagnetic CDW orders, $\sqrt{3} \times \sqrt{3}$ and $2 \times 2\sqrt{3}$ CDWs, can be generated in ML- VSe_2 under certain critical ϵ . Importantly, the momentum-dependent electron-phonon coupling (MEPC) and FSN, the major driving forces for forming these two ferromagnetic CDWs, are strongly spin dependent, eventually satisfying criterion (iii). Consequently, the $\sqrt{3} \times \sqrt{3}$ and $2 \times 2\sqrt{3}$ CDWs exhibit fascinating half-metallic phases under a large range of ϵ . In particular, the $\sqrt{3} \times \sqrt{3}$ CDW possesses an A-type half-metallic state with a flat band around E_F , whereas the $2 \times 2\sqrt{3}$ CDW holds a B-type half-metallic state with a clean Dirac cone at E_F .

III. GENERATING FERROMAGNETIC CDWs IN ML- VSe_2

The structure of ML $1T$ - VSe_2 has a space group of $P\bar{3}m1$, where one V layer is sandwiched by two Se layers. The calculated lattice constant of ML $1T$ - VSe_2 (3.34 Å) agrees well with the experimentally measured one (~ 3.35 Å) [21]. Without an external field, the ferromagnetic $1T$ phase is the ground state, whose total energy is ~ 24 meV/f.u. lower than that of the nonmagnetic one. This ferromagnetic $1T$ phase has been observed by some experiments at room temperature [20,21]. On the other hand, the phonon spectrum of the nonmagnetic $1T$ phase shows a strong instability with imaginary phonon modes near $1/2 \Gamma$ - M and $3/5 \Gamma$ - K (Fig. S1 [31]), indicating the existence of 4×4 and $\sqrt{7} \times \sqrt{3}$ CDWs (Table S1 [31]), respectively. Indeed, these nonmagnetic CDWs have also been observed in experiments [14–19]. Importantly, the calculated total energy of the ferromagnetic $1T$ phase is ~ 13.8 and ~ 11.7 meV/f.u. lower than that of nonmagnetic 4×4 and $\sqrt{7} \times \sqrt{3}$ CDWs, respectively, which indicates that ML- VSe_2 meets criterion (i) for forming ferromagnetic CDWs.

To check whether criterion (ii) can be simultaneously satisfied, we have further calculated the energy and dynamic instability of the ferromagnetic $1T$ phase under the external strain field. As shown in Fig. 2(a), the energy difference (ΔE) between the ferromagnetic $1T$ phase and these two nonmagnetic CDWs increases (decreases) as a function of tensile (compressive) ϵ , indicating that the energetic stability of the corresponding ferromagnetic $1T$ phase can be enhanced under tensile ϵ . Surprisingly, when tensile ϵ is applied, although the total energy of the ferromagnetic $1T$ phase can be further lowered compared with the nonmagnetic CDWs, its dynamic instability increases, as indicated by the calculated phonon spectra in Fig. 2(b). The larger the ϵ , the softer are the phonon modes. Therefore, ML- VSe_2 can also meet criterion (ii) for

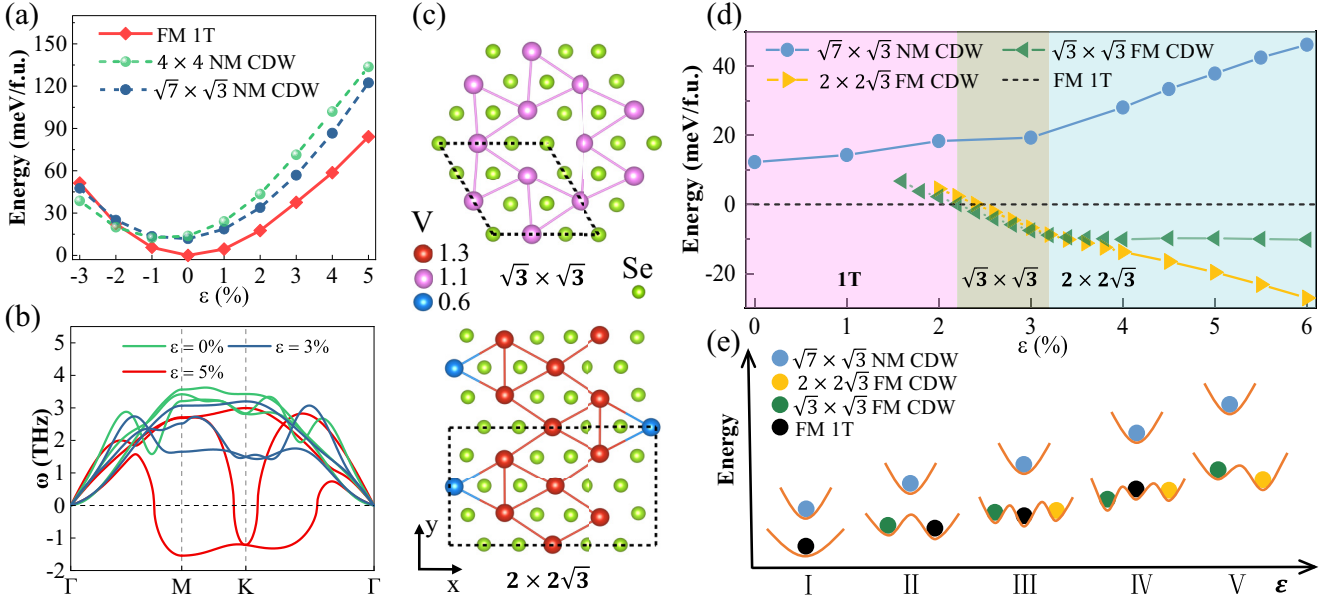


FIG. 2. Strain-tunable ferromagnetic CDWs in ML-VSe₂. (a) Calculated total energies of FM 1T phase and two NM CDWs in ML-VSe₂ as a function of strain. (b) Lowest three branches of FM 1T phase phonon spectra under three typical tensile strains. (c) Top views of $\sqrt{3} \times \sqrt{3}$ ($\epsilon = 3\%$) and $2 \times 2\sqrt{3}$ ($\epsilon = 5\%$) configurations. Primitive cells are marked as dashed lines. Variable magnetic moments in V atoms are illustrated with different colors (in units of μ_B). (d) The total energies of FM 1T and various CDW phases as a function of tensile strain. (e) Energy diagram of strain-tunable CDW phase transitions.

forming ferromagnetic CDWs. Particularly, when $\epsilon = 5\%$, two imaginary phonon modes appear, i.e., one is located along M - K - Γ and the other is located at K . The maximum at M (K) suggests a 2×2 ($\sqrt{3} \times \sqrt{3}$) CDW, while the maximum near $3/4$ Γ - K suggests a $2 \times 2\sqrt{3}$ CDW (Table S1 [31]).

While it is found that the 2×2 CDW is dynamically unstable with a spontaneous transformation to a $2 \times 2\sqrt{3}$ CDW within a doubled supercell, both $2 \times 2\sqrt{3}$ and $\sqrt{3} \times \sqrt{3}$ CDWs are dynamically stable under tensile strain (Fig. S2 [31]). Importantly, the ferromagnetic order of both CDWs can survive the formation of a CDW. As shown in Fig. 2(c), the $\sqrt{3} \times \sqrt{3}$ CDW (space group $P3m1$) is formed by the antitramerization of V atoms in the 1T phase while the $2 \times 2\sqrt{3}$ CDW (space group $P2_1$) is formed by the reconstruction of V atoms into a zigzag stripe. In addition, the local magnetic moments of V atoms are uniformly distributed in a $\sqrt{3} \times \sqrt{3}$ CDW but exhibit a spin oscillation along the x axis in the $2 \times 2\sqrt{3}$ CDW [Fig. 2(c)].

In Fig. 2(d), we have calculated the total energies of these ferromagnetic CDWs as a function of tensile ϵ , compared with the ferromagnetic 1T phase and nonmagnetic $\sqrt{7} \times \sqrt{3}$ CDW. Interestingly, ϵ -tunable multiple phase transitions between ferromagnetic 1T and ferromagnetic CDWs are observed. When $0 \leq \epsilon < 1.8\%$, the ferromagnetic 1T phase is the ground state, while ferromagnetic CDWs cannot exist [I in Fig. 2(e)]. When $1.8 \leq \epsilon < 2\%$, the $\sqrt{3} \times \sqrt{3}$ CDW appears as a metastable state [II in Fig. 2(e)]. When $2 \leq \epsilon < 2.2\%$, a $2 \times 2\sqrt{3}$ CDW emerges as another metastable state [III in Fig. 2(e)]. Importantly, when $2.2 \leq \epsilon < 3.2\%$, the first ground state phase transition occurs from 1T to $\sqrt{3} \times \sqrt{3}$ CDW [IV in Fig. 2(e)], i.e., the ferromagnetic CDW is now stabilized as the ground state. When $\epsilon \geq 3.2\%$, the second

ground state phase transition occurs from $\sqrt{3} \times \sqrt{3}$ CDW to $2 \times 2\sqrt{3}$ CDW; meanwhile, the 1T phase is no longer a metastable state [V in Fig. 2(e)]. On the other hand, the ΔE between the nonmagnetic $\sqrt{7} \times \sqrt{3}$ CDW and these two ferromagnetic CDWs increases as ϵ increases, i.e., the larger the ϵ , the stronger is the instability of the nonmagnetic CDW.

We have further confirmed the energetic stability of ferromagnetic orders in $\sqrt{3} \times \sqrt{3}$ and $2 \times 2\sqrt{3}$ CDWs by comparing them with other typical antiferromagnetic orders (Fig. S3 and Table S2 [31]). It turns out that ferromagnetic orders are always energetically favorable for both $\sqrt{3} \times \sqrt{3}$ and $2 \times 2\sqrt{3}$ CDWs under tensile strain. The larger ϵ results in more stable ferromagnetic orders. Interestingly, the calculated magnetocrystalline anisotropy energy (MAE) shows that the easy axis of ferromagnetic CDWs is along the in-plane direction, similar to CrCl₃ [32]; and the larger the ϵ , the larger is the MAE. These results indicate that a larger ϵ can induce a higher T_c in these ferromagnetic CDWs with T_c much higher than TaS₂.

IV. ELECTRONIC STRUCTURES OF FERROMAGNETIC CDWs

It is important to further understand the electronic structures of these two ferromagnetic CDWs. Here, the spin-polarization ratio P is defined as $P = [N_{\uparrow}(E_F) - N_{\downarrow}(E_F)] / [N_{\uparrow}(E_F) + N_{\downarrow}(E_F)]$ [33], where $N_{\uparrow}(E_F)$ and $N_{\downarrow}(E_F)$ are the DOS values at E_F in the spin \uparrow (majority) and spin \downarrow (minority) channels, respectively. The calculated ϵ -dependent P for ground states is summarized in Fig. 3(a). When $0 \leq \epsilon < 2.2\%$, the P of the ferromagnetic 1T phase is very small ($\sim 10\%$) and insensitive to ϵ . Remarkably, when $2.2 \leq$

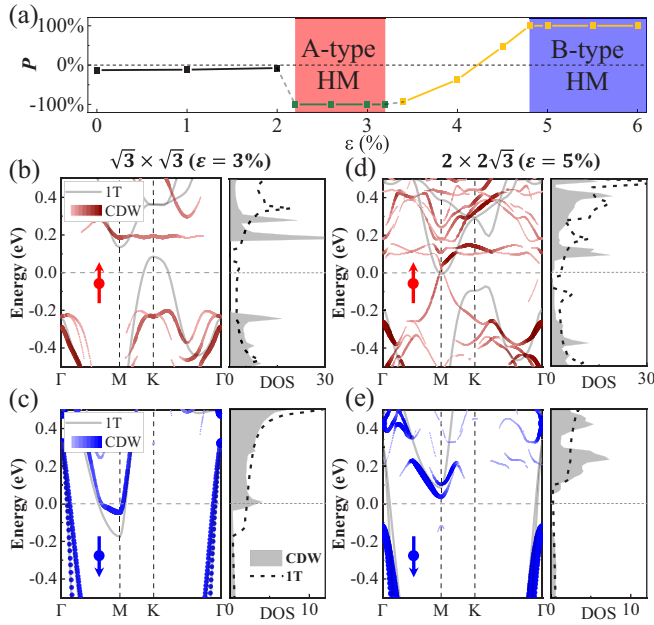


FIG. 3. Electronic structures of ferromagnetic CDWs. (a) Spin-polarization ratio P as a function of strain for different ground states. Unfolded band structures and DOS for $\sqrt{3} \times \sqrt{3}$ CDW ($\varepsilon = 3\%$) in (b) spin \uparrow and (c) spin \downarrow channels. (d), (e) Same as (b) and (c) but for $2 \times 2\sqrt{3}$ CDW ($\varepsilon = 5\%$). Band structures of FM 1T-VSe₂ are also plotted here for comparison. The Fermi level is set to zero.

$\varepsilon < 3.2\%$, the P of $\sqrt{3} \times \sqrt{3}$ CDW remains -100% , denoted as A-type half-metallicity [the majority (minority) spin channel is insulating (metallic)]. When $3.2 \leq \varepsilon < 4.8\%$, the band gap in the spin \uparrow (\downarrow) channel of the $2 \times 2\sqrt{3}$ CDW gradually decreases (increases) (Fig. S4 [31]), along with P gradually changing from $\sim -90\%$ to 100% . When $\varepsilon \geq 4.8\%$, the P of the $2 \times 2\sqrt{3}$ CDW remains 100% , denoted as B-type half-metallicity [the majority (minority) spin channel is conducting (insulating)]. In practice, these two different types of half-metallic phases can be distinguishable using the spin-resolved scanning tunneling microscopy (STM) measurements (see Fig. S5 [31] and the related discussion).

In the following, the $\sqrt{3} \times \sqrt{3}$ ($\varepsilon = 3\%$) and $2 \times 2\sqrt{3}$ ($\varepsilon = 5\%$) CDWs are selected to explore their unusual half-metallic states. For $\sqrt{3} \times \sqrt{3}$ CDW, in the spin \uparrow channel [Fig. 3(b)], the hole pocket centered at K in the FM 1T phase is largely suppressed and pushed down to a lower-energy position during CDW formation, forming a Mexican-hat-shaped band dispersion with a large DOS peak at the valence band maximum (VBM). Importantly, the strong band renormalization results in an unusual flat band, composed of twofold Vd orbitals, in the bottom of the conduction band along M - K - Γ , reflected by the very sharp DOS peak at the conduction band minimum (CBM). The formation of this flat band might be due to the antitrimerization of V atoms in a triangularlike frustrated lattice [34]. Furthermore, this flat band can gradually shift down to E_F under larger tensile ε and electron doping (Fig. S6 [31]). In the spin \downarrow channel [Fig. 3(c)], the energy bands are much less changed during the CDW formation, i.e., the electron pocket centered at M is slightly pushed up. Eventually, an A-type half-metallic phase is formed. Interest-

ingly, DOS at E_F in the spin \uparrow (\downarrow) channel is fully suppressed (remarkably increased) during the $\sqrt{3} \times \sqrt{3}$ CDW formation, invalidating the common expectation that CDW formation is accompanied by a DOS reduction at E_F [35–37]. This highly asymmetrical band renormalization in the spin \uparrow and \downarrow channels results in a large half-metallic band gap ~ 0.4 eV.

Figures 3(d) and 3(e) show the calculated spin \uparrow and \downarrow band structures of $2 \times 2\sqrt{3}$ CDWs, respectively. A larger band renormalization also occurs in the spin \uparrow channel than in the spin \downarrow channel during CDW formation, along with largely reduced (fully suppressed) DOS at E_F in the spin \uparrow (\downarrow) channel. Accordingly, a B-type half-metallic phase with an insulating state located in the spin \downarrow channel is formed in the $2 \times 2\sqrt{3}$ CDW. Unexpectedly, as shown in Fig. 3(d), a clean Dirac cone located at M around E_F appears in the unfolded band structure of the spin \uparrow channel, accompanied by the suppression of a local band gap during CDW formation, which may be visible under spin-resolved angle-resolved photoemission spectroscopy (ARPES) measurements [38]. In the spin \downarrow channel [Fig. 3(e)], the hole pocket centered at Γ is strongly pushed down by ~ 0.4 eV, which not only plays a key role in forming a half-metallic band gap ~ 0.2 eV but also introduces a new valley state around Γ .

V. ORIGINS OF FERROMAGNETIC CDWs UNDER STRAIN

The driving force behind the CDW transition is an important subject with an ongoing controversy [4,39,40]. The strong spin-dependent band renormalization in $\sqrt{3} \times \sqrt{3}$ and $2 \times 2\sqrt{3}$ CDWs indicates that the driving force for these CDW formations may have a strong spin dependence feature. Generally, FSN and/or MEPC, common origins of the observed CDWs in many TMD systems [3,13], are spin independent. The real ($\text{Re } \chi$) and imaginary ($\text{Im } \chi$) parts of electron susceptibility χ reflect the electron instability and FSN of a system [39], respectively. When both $\text{Re } \chi$ and $\text{Im } \chi$ peak at the same wave vector \mathbf{q} , a CDW induced by FSN with \mathbf{q}_{CDW} may be triggered. Furthermore, MEPC can be evaluated by calculating the phonon linewidth γ [41].

Figure 4 shows the calculated spin-resolved $\text{Im } \chi$ and γ of ferromagnetic 1T-VSe₂ under two typical ε , which indeed exhibit a strong spin dependence, satisfying criterion (iii) for forming half-metallic CDWs. For $\varepsilon = 3\%$, as shown in Fig. 4(a) and Fig. S7 [31], noticeable peaks appear around K in both $\text{Re } \chi$ and $\text{Im } \chi$ of the spin \uparrow channel, but not of the spin \downarrow channel. Contributed by the hole pocket around K [Fig. 3(b)], FSN of the spin \uparrow channel rather than the spin \downarrow channel could contribute to the formation of half-metallic $\sqrt{3} \times \sqrt{3}$ CDWs (Table S1 [31]). In addition, it may also provide a valid understanding of the much larger band renormalization in the spin \uparrow [Fig. 3(b)] than in the spin \downarrow [Fig. 3(c)] channel, a key factor for forming half metallicity. Meanwhile, as shown in Fig. 4(b), high-intensity peaks of γ appear around K in both spin channels, suggesting that MEPC may be another possible reason to form half-metallic $\sqrt{3} \times \sqrt{3}$ CDWs. Therefore, the joint MEPC and (spin-dependent) FSN may contribute to the half-metallic $\sqrt{3} \times \sqrt{3}$ CDW formation.

The situation is different for $\varepsilon = 5\%$. A hole pocket around K [Fig. 3(b)] of the spin \uparrow channel in the ferromagnetic 1T phase under $\varepsilon = 3\%$ is now converted to an electron pocket at

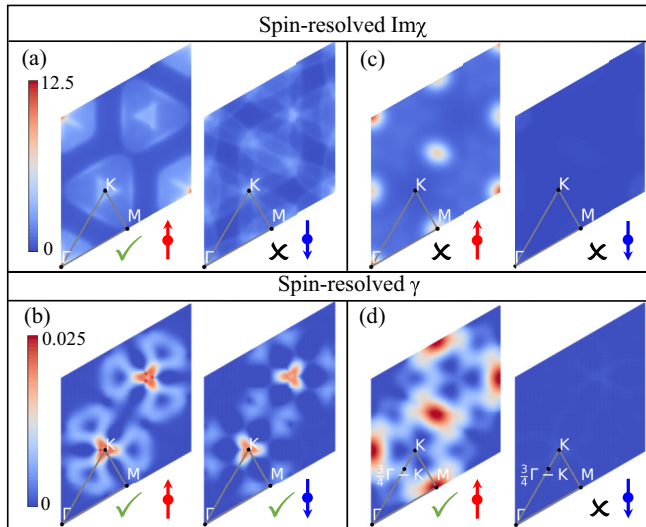


FIG. 4. Origins of strain-dependent ferromagnetic CDWs. (a) Spin-resolved $\text{Im}\chi$ and (b) γ (contributed by the lowest phonon mode in the phonon spectrum) for FM $1T$ -VSe₂ under $\varepsilon = 3\%$. (c), (d) Same as (a) and (b) but under $\varepsilon = 5\%$. The unit of γ is THz.

M at FS [Fig. 3(d)], changing the FSN condition dramatically. Indeed, as shown in Fig. 4(c), the peak in $\text{Im}\chi$ shifts from K to M in the spin \uparrow channel, which, unfortunately, cannot contribute to the $2 \times 2\sqrt{3}$ CDW formation (Table S1 [31]). In the spectra of γ [Fig. 4(d)], we can observe three distinctive peaks around M , $3/4 \Gamma$ - K , and K in the spin \uparrow channel. The peak at $3/4 \Gamma$ - K in the spin \uparrow channel indicates that the key driving force to form half-metallic $2 \times 2\sqrt{3}$ CDWs may be MEPC. Meanwhile, no noticeable peaks are observed in both $\text{Im}\chi$ and γ in the spin \downarrow channel. This may account for the observed larger band renormalization in the spin \uparrow [Fig. 3(d)] than in the spin \downarrow [Fig. 3(e)] channel. Hence, the spin-selective MEPC, rather than FSN, may play a major role in forming half-metallic $2 \times 2\sqrt{3}$ CDWs. Figure 4 reveals the

unusual relationship between the CDW transition and half-metallicity formation.

VI. OUTLOOK

In the current experiments, some popular substrates with smaller lattice constants than ML-VSe₂ are frequently applied for growing ML-VSe₂ [16,18–20]. It might induce some compressive ε to ML-VSe₂, effectively suppressing the energetic stability of ferromagnetic order and even stabilizing the nonmagnetic CDWs as ground states [Fig. 2(a)]. To meet the criteria to form ferromagnetic CDWs, we suggest that the ML-VSe₂ should be prepared on the substrates with a larger lattice constant, or directly apply tensile strain, e.g., via bending [42]. It seems quite difficult to apply such a large strain experimentally. However, the stress cost for 5% tensile strain in VSe₂ is less than the experimentally realized $\sim 1\%$ strain for graphene [43] and $\sim 1.8\%$ strain for MoS₂ [44] (see Fig. S10 and the related discussion [31]). In general, our strategy for generating ferromagnetic CDWs is valid in many other 2D systems (such as VS₂) under various external fields, not limited to strain fields.

It is worth noting that both nonmagnetic CDWs and magnetism in bulk are much different from monolayers in $1T$ -VSe₂. Therefore, further research on examining whether our conclusions would change in a bulk state or few-layer form is encouraged. In addition, theoretical treatments of this system with beyond-mean-field theory and experimental observations are also eagerly needed to confirm our predicted structures and properties of ferromagnetic CDWs.

ACKNOWLEDGMENTS

The authors thank Professor Zheng Liu and Professor Ying-Shuang Fu for their helpful discussions. This work is supported by the NSFC (Grant No. 12088101) and NSF (Grant No. U1930402). Computations are done at the Tianhe-JK supercomputer at CSRC.

- [1] T. Kiss, T. Yokoya, A. Chainani, S. Shin, T. Hanaguri, M. Nohara, and H. Takagi, *Nat. Phys.* **3**, 720 (2007).
- [2] M. M. Ugeda, A. J. Bradley, Y. Zhang, S. Onishi, Y. Chen, W. Ruan, C. Ojeda-Aristizabal, H. Ryu, M. T. Edmonds, H.-Z. Tsai, A. Riss, S.-K. Mo, D. Lee, A. Zettl, Z. Hussain, Z.-X. Shen, and M. F. Crommie, *Nat. Phys.* **12**, 92 (2016).
- [3] S. Manzeli, D. Ovchinnikov, D. Pasquier, O. V. Yazyev, and A. Kis, *Nat. Rev. Mater.* **2**, 17033 (2017).
- [4] B.-X. Zheng, C.-M. Chung, P. Corboz, G. Ehlers, M.-P. Qin, R. M. Noack, H. Shi, S. R. White, S. Zhang, and G. K.-L. Chan, *Science* **358**, 1155 (2017).
- [5] T. Neupert, M. M. Denner, J.-X. Yin, R. Thomale, and M. Z. Hasan, *Nat. Phys.* **18**, 137 (2022).
- [6] C. Mielke, D. Das, J.-X. Yin, H. Liu, R. Gupta, Y.-X. Jiang, M. Medarde, X. Wu, H. C. Lei, J. Chang, P. Dai, Q. Si, H. Miao, R. Thomale, T. Neupert, Y. Shi, R. Khasanov, M. Z. Hasan, H. Luetkens, and Z. Guguchia, *Nature (London)* **602**, 245 (2022).
- [7] M. Kratochvilova, A. D. Hillier, A. R. Wildes, L. Wang, S.-W. Cheong, and J.-G. Park, *npj Quantum Mater.* **2**, 42 (2017).
- [8] S.-Y. Yang, Y. Wang, B. R. Ortiz, D. Liu, J. Gayles, E. Derunova, R. Gonzalez-Hernandez, L. Šmejkal, Y. Chen, S. S. P. Parkin, S. D. Wilson, E. S. Toberer, T. McQueen, and M. N. Ali, *Sci. Adv.* **6**, eabb6003 (2020).
- [9] V. Vaňo, M. Amini, S. C. Ganguli, G. Chen, J. L. Lado, S. Kezilebieke, and P. Liljeroth, *Nature (London)* **599**, 582 (2021).
- [10] I. Žutić, J. Fabian, and S. D. Sarma, *Rev. Mod. Phys.* **76**, 323 (2004).
- [11] M. Yoshida, R. Suzuki, Y. Zhang, M. Nakano, and Y. Iwasa, *Sci. Adv.* **1**, e1500606 (2015).
- [12] S.-K. Chan and V. Heine, *J. Phys. F: Met. Phys.* **3**, 795 (1973).
- [13] K. Rossnagel, *J. Phys.: Condens. Matter* **23**, 213001 (2011).
- [14] D. Zhang, J. Ha, H. Baek, Y.-H. Chan, F. D. Natterer, A. F. Myers, J. D. Schumacher, W. G. Cullen, A. V. Davydov, Y. Kuk, M. Y. Chou, N. B. Zhitenev, and J. A. Stroscio, *Phys. Rev. Mater.* **1**, 024005 (2017).

- [15] P. Chen, W. W. Pai, Y.-H. Chan, V. Madhavan, M. Y. Chou, S.-K. Mo, A.-V. Fedorov, and T.-C. Chiang, *Phys. Rev. Lett.* **121**, 196402 (2018).
- [16] J. Feng, D. Biswas, A. Rajan, M. D. Watson, F. Mazzola, O. J. Clark, K. Underwood, I. Marković, M. McLaren, A. Hunter, D. M. Burn, L. B. Duffy, S. Barua, G. Balakrishnan, F. Bertran, P. L. Fèvre, T. K. Kim, G. van der Laan, T. Hesjedal, P. Wahl, and P. D. C. King, *Nano Lett.* **18**, 4493 (2018).
- [17] G. Duvjir, B. K. Choi, I. Jang, S. Ulstrup, S. Kang, T. T. Ly, S. Kim, Y. H. Choi, C. Jozwiak, A. Bostwick, E. Rotenberg, J.-G. Park, R. Sankar, K.-S. Kim, J. Kim, and Y. J. Chang, *Nano Lett.* **18**, 5432 (2018).
- [18] A. O. Fumega, M. Gobbi, P. Dreher, W. Wan, C. González-Orellana, M. Peña-Díaz, C. Rogero, J. Herrero-Martín, P. Gargiani, M. Ilyn, M. M. Ugeda, V. Pardo, and S. Blanco-Canosa, *J. Phys. Chem. C* **123**, 27802 (2019).
- [19] P. M. Coelho, K. N. Cong, M. Bonilla, S. Kolekar, M.-H. Phan, J. Avila, M. C. Asensio, I. I. Oleynik, and M. Batzill, *J. Phys. Chem. C* **123**, 14089 (2019).
- [20] M. Bonilla, S. Kolekar, Y. Ma, H. C. Diaz, V. Kalappattil, R. Das, T. Eggers, H. R. Gutierrez, M.-H. Phan, and M. Batzill, *Nat. Nanotechnol.* **13**, 289 (2018).
- [21] W. Yu, J. Li, T. S. Herng, Z. Wang, X. Zhao, X. Chi, W. Fu, I. Abdelwahab, J. Zhou, J. Dan, Z. Chen, Z. Chen, Z. Li, J. Lu, S. J. Pennycook, Y. P. Feng, J. Ding, and K. P. Loh, *Adv. Mater.* **31**, 1903779 (2019).
- [22] T. Yilmaz, E. Vescovo, J. T. Sadowski, and B. Sinkovic, *Phys. Rev. B* **105**, 245114 (2022).
- [23] C. van Bruggen and C. Haas, *Solid State Commun.* **20**, 251 (1976).
- [24] R. Chua, J. Henke, S. Saha, Y. Huang, J. Gou, X. He, T. Das, J. van Wezel, A. Soumyanarayanan, and A. T. S. Wee, *ACS Nano* **16**, 783 (2022).
- [25] C. Lee, X. Wei, J. W. Kysar, and J. Hone, *Science* **321**, 385 (2008).
- [26] F. Guinea, M. I. Katsnelson, and A. K. Geim, *Nat. Phys.* **6**, 30 (2010).
- [27] K. S. Novoselov, A. K. Geim, S. V. Morozov, D. Jiang, Y. Zhang, S. V. Dubonos, I. V. Grigorieva, and A. A. Firsov, *Science* **306**, 666 (2004).
- [28] Y. Zhang, T.-T. Tang, C. Girit, Z. Hao, M. C. Martin, A. Zettl, M. F. Crommie, Y. R. Shen, and F. Wang, *Nature (London)* **459**, 820 (2009).
- [29] S. Cho, S. Kim, J. H. Kim, J. Zhao, J. Seok, D. H. Keum, J. Baik, D.-H. Choe, K. J. Chang, K. Suenaga, S. W. Kim, Y. H. Lee, and H. Yang, *Science* **349**, 625 (2015).
- [30] Z. Sun, A. Martinez, and F. Wang, *Nat. Photon.* **10**, 227 (2016).
- [31] See Supplemental Material at <http://link.aps.org/supplemental/10.1103/PhysRevB.106.165112> for more information about the computational method, relation between the CDW supercell and primitive cell, phonon spectrum of NM 1T phase and FM CDWs, antiferromagnetic (AFM) configurations, electronic structure of FM CDWs, real part of electron susceptibility, and full STM simulation images, which includes Refs. [45–55].
- [32] A. Bedoya-Pinto, J.-R. Ji, A. K. Pandeya, P. Gargiani, M. Valvidares, P. Sessi, J. M. Taylor, F. Radu, K. Chang, and S. S. P. Parkin, *Science* **374**, 616 (2021).
- [33] Y. Sun, Z. Zhuo, X. Wu, and J. Yang, *Nano Lett.* **17**, 2771 (2017).
- [34] D. Călugăru, A. Chew, L. Elcoro, Y. Xu, N. Regnault, Z.-D. Song, and B. A. Bernevig, *Nat. Phys.* **18**, 185 (2022).
- [35] C.-S. Lian, C. Si, and W. Duan, *Nano Lett.* **18**, 2924 (2018).
- [36] H. Tan, Y. Liu, Z. Wang, and B. Yan, *Phys. Rev. Lett.* **127**, 046401 (2021).
- [37] S. Seong, H. Kim, K. Kim, B. I. Min, Y. S. Kwon, S. W. Han, B.-G. Park, R. Stania, Y. Seo, and J.-S. Kang, *Phys. Rev. B* **104**, 195153 (2021).
- [38] B. Lv, T. Qian, and H. Ding, *Nat. Rev. Phys.* **1**, 609 (2019).
- [39] M. D. Johannes and I. I. Mazin, *Phys. Rev. B* **77**, 165135 (2008).
- [40] X. Zhu, Y. Cao, J. Zhang, E. W. Plummer, and J. Guo, *Proc. Natl. Acad. Sci. USA* **112**, 2367 (2015).
- [41] J. Diego, A. H. Said, S. K. Mahatha, R. Bianco, L. Monacelli, M. Calandra, F. Mauri, K. Rossnagel, I. Errea, and S. Blanco-Canosa, *Nat. Commun.* **12**, 598 (2021).
- [42] E. Han, J. Yu, E. Annevelink, J. Son, D. A. Kang, K. Watanabe, T. Taniguchi, E. Ertekin, P. Y. Huang, and A. M. van der Zande, *Nat. Mater.* **19**, 305 (2020).
- [43] J. Zabel, R. R. Nair, A. Ott, T. Georgiou, A. K. Geim, K. S. Novoselov, and C. Casiraghi, *Nano Lett.* **12**, 617 (2012).
- [44] Y. Zhang, M.-K. Choi, G. Haugstad, E. B. Tadmor, and D. J. Flannigan, *ACS Nano* **15**, 20253 (2021).
- [45] K. Kunc and R. M. Martin, *Phys. Rev. Lett.* **48**, 406 (1982).
- [46] P. E. Blöchl, *Phys. Rev. B* **50**, 17953 (1994).
- [47] G. Kresse and J. Furthmüller, *Phys. Rev. B* **54**, 11169 (1996).
- [48] J. P. Perdew, K. Burke, and M. Ernzerhof, *Phys. Rev. Lett.* **77**, 3865 (1996).
- [49] P. Giannozzi, S. Baroni, N. Bonini, M. Calandra, R. Car, C. Cavazzoni, D. Ceresoli, G. L. Chiarotti, M. Cococcioni, I. Dabo, A. D. Corso, S. de Gironcoli, S. Fabris, G. Fratesi, R. Gebauer, U. Gerstmann, C. Gougoussis, A. Kokalj, M. Lazzeri, L. Martin-Samos *et al.*, *J. Phys.: Condens. Matter* **21**, 395502 (2009).
- [50] R. Wiesendanger, *Rev. Mod. Phys.* **81**, 1495 (2009).
- [51] P. V. C. Medeiros, S. Stafström, and J. Björk, *Phys. Rev. B* **89**, 041407(R) (2014).
- [52] A. A. Mostofi, J. R. Yates, G. Pizzi, Y.-S. Lee, I. Souza, D. Vanderbilt, and N. Marzari, *Comput. Phys. Commun.* **185**, 2309 (2014).
- [53] A. Togo and I. Tanaka, *Scr. Mater.* **108**, 1 (2015).
- [54] P. V. C. Medeiros, S. S. Tsirkin, S. Stafström, and J. Björk, *Phys. Rev. B* **91**, 041116(R) (2015).
- [55] J. G. Si, W. J. Lu, H. Y. Wu, H. Y. Lv, X. Liang, Q. J. Li, and Y. P. Sun, *Phys. Rev. B* **101**, 235405 (2020).